Available online at www.sciencedirect.com
SCIENCE DIRECT
ELSEVIER
Journal of the European Ceramic Society 26 (2006) 501–507
ECERS
www.elsevier.com/locate/jeurceramsoc

Syntheses of calcium-deficient apatite fibres by a homogeneous precipitation method and their characterizations

Mamoru Aizawa [a,*], Hiroko Ueno [b], Kiyoshi Itatani [b], Isao Okada [b]

[a] *Department of Industrial Chemistry, School of Science and Technology, Meiji University, Kanagawa 214-8571, Japan*
[b] *Department of Chemistry, Faculty of Science and Engineering, Sophia University, Chiyoda-ku, Tokyo 102-8554, Japan*

Available online 10 August 2005

Abstract

Calcium-deficient apatite fibres were successfully synthesized by a homogeneous precipitation method using starting solutions with a Ca/P ratio of 1.00–1.67. In the case of the Ca/P ratio of 1.67, the resulting apatite fibre had long-axes of about 60–100 μm and contained 5.2 mass % of carbonate ions. The Ca/P ratio of apatite fibres could be controlled in the range of 1.53–1.68 by changing the Ca/P ratio of the starting solutions from 1.00 to 1.67. The long-axes and the carbonate contents of the resulting calcium-deficient apatite fibres increased with Ca/P ratio of the starting solutions. These apatite fibres were of single crystal and had a preferred orientation in the *c*-axis direction.

Keywords: Powder-chemical preparation; Fibres; Apatite; Biomedical applications; Calcium-deficient hydroxyapatite

1. Introduction

Hydroxyapatite ($Ca_{10}(PO_4)_6(OH)_2$; HAp) has been widely applied as a biomaterial for substituting human hard tissues,[1,2] and as an adsorbent for chromatography.[3] The HAp crystal has two types of crystal planes, bearing different charges: positive on the *a*-planes and negative on the *c*-planes.[3] Thus, novel properties may be produced by controlling the orientation of the crystal planes. Controlled orientation may be achieved by modifying the morphology of HAp crystals. For example, in order to increase the positive charge on the surface of the HAp fibres, one can grow hexagonal-shaped HAp fibres which are oriented along the *c*-axis so that the *a*(*b*)-plane is wider than the *c*-plane. These apatite fibres have specific adsorptions to negatively charged acidic proteins.

The morphological control of HAp crystals has been reported previously by some researchers. For example, Ioku et al.[4] synthesized apatite whiskers with a long-axis of several micrometers in length by a hydrothermal process and demonstrated by transmission electron microscopy (TEM) that the whiskers were of single crystal. On the other hand, Yokogawa et al.[5] synthesized the plate-shaped apatites by a hydrothermal process in the presence of organic solvents.

We have also successfully synthesized apatite fibres with long axes of 60–100 μm by homogeneous precipitation method.[6,7] It was confirmed from the results of high-resolution transmission electron microscopy (HR-TEM) using a shadow imaging technique that the apatite fibres were of single crystals with the *c*-axis orientation parallel to the long axis of the fibre.[8,9]

Using the above fibres, we have promoted the development of (i) porous HAp ceramics with well-controlled pore sizes[7,10] and (ii) HAp/polymer hybrids possessing mechanical properties similar to those of living cortical bone by in situ bulk polymerization of the monomer in the pores of the ceramic.[11] This hybrid, with mechanical properties similar to those of cortical bone, has been shown to have excellent biocompatibility both in vitro and in vivo.[12,13] In addition, we have developed a three-dimensional scaffold with large interconnected pores of 100–250 μm in diameter and high porosities of 98–99% for tissue engineering of bone from the above-mentioned apatite fibres.[14–16] We have already clarified that the apatite-fibre scaffold has an excellent cellular response, such as enhanced differentiation to osteoblasts.

* Corresponding author. Tel.: +81 44 934 7237; fax: +81 44 934 7906.
E-mail address: mamorua@isc.meiji.ac.jp (M. Aizawa).

0955-2219/$ – see front matter © 2005 Elsevier Ltd. All rights reserved.
doi:10.1016/j.jeurceramsoc.2005.07.007

On the other hands, the constituent ions of HAp crystals can be replaced by many other kinds of ions while maintaining the skeleton, leading to form various substituted apatite compounds.[17] Calcium-deficient hydroxyapatite (Ca-def HAp), $Ca_{10-x}(HPO_4)_x(PO_4)_{6-x}(OH)_{2-x}{\cdot}nH_2O$, belongs to the apatite family.[18] It is well-known that Ca-def HAp has higher chemical activity than pure HAp and forms biodegradable tricalcium phosphate ($Ca_3(PO_4)_2$; TCP)[19] or TCP/HAp biphase by thermal decomposition. Thus, Ca-def HAp may be expected as a starting material to prepare biodegradable bioceramics.

If one can control the Ca/P ratio of the above-mentioned apatite fibres, the fibre-derived bioceramics may have a well-controlled chemical composition. For example, Ca-def HAp fibre with a Ca/P ratio of 1.50 will produce the TCP phase after heat treatment. The aims of the present investigation were to synthesize Ca-def HAp fibres with the controlled Ca/P ratios and to examine some properties, including particle morphology and thermal stability, of the resulting fibres using some suitable techniques.

2. Experimental

2.1. Syntheses of calcium-deficient apatite fibres

Ca-def HAp fibres were synthesized by partly modifying the apatite-fibre processing previously reported.[7] Ten kinds of starting solutions with the Ca/P ratios of 1.00–1.67 were prepared by mixing the 0.100–0.167 mol dm^{-3} $Ca(NO_3)_2$, 0.100 mol dm^{-3} $(NH_4)_2HPO_4$, 0.500 mol dm^{-3} $(NH_2)_2CO$ and 0.10 mol dm^{-3} HNO_3 aqueous solutions. Concentrations of Ca^{2+} ion in the starting solution were 0.100, 0.110, 0.120, 0.130, 0.140, 0.150, 0.155, 0.160, 0.164 and 0.167 mol dm^{-3}.

Each starting solution (0.5 dm^3) was refluxed at 80 °C for 24 h to form octacalcium phosphate ($Ca_8H_2(PO_4)_6{\cdot}5H_2O$; OCP) via $CaHPO_4$ and then the resulting OCP was converted into HAp by refluxing at 90 °C for 72 h. The pH in the solution increased from ~3 to ~8, owing to the NH_3 formed by the hydrolysis of the urea as a precipitating agent. The products were composed of fibre-shaped particles and granules. The fibre fractions were easily separated by decantation; the yield of the fibre was in range of 50–60%.

2.2. Characterization of the resulting calcium-deficient apatite fibres

The crystalline phases of the powders were identified using an X-ray powder diffractometer (XRD; RINT2000PC, Rigaku; 40 kV, 40 mA). The lattice constants were calculated by the least-squares method using the JADE program attached to RINT2000PC. Fourier transform infrared spectroscopy (FT-IR) was performed using Shimadzu 8200, the measuring range of which was 400–4000 cm^{-1}.

The contents of calcium and phosphorus in each fibre were determined using an inductively coupled plasma emission spectrometer (ICP-ES; Seiko, SPS-7700). The contents of carbon in the fibre were measured using an element analyzer (PE2400-II, Perkin–Elmer).

The morphologies were observed using a scanning electron microscope (SEM; Hitachi, S-4500) and a TEM (JEOL, CX200). TEM samples were prepared by dispersing the fibres in ethanol and collecting them onto Cu mesh TEM grids.

2.3. Thermal stability of the resulting calcium-deficient apatite fibres

The differential thermal analysis and thermogravimetry (DTA-TG; Rigaku, Thermo Plus TG8120) were carried out using about 15 mg of the fibre at a heating rate of 10 °C min^{-1}. In addition, we performed XRD measurement of the fibre heated at 1200 °C for 1 h.

3. Results and discussion

3.1. Syntheses of calcium-deficient apatite fibres and their characterizations

Fig. 1 shows the XRD patterns for the products from typical starting solutions with various Ca/P ratios. In the case of the Ca/P = 1.67 of the starting solution (Fig. 1(a)), the HAp was present in the sample powder, and the (1 0 0), (2 0 0) and (300) reflections of the resulting apatite were more intense than those of the typical HAp listed in JCPDS card #9–432. The XRD pattern changed to the typical HAp pat-

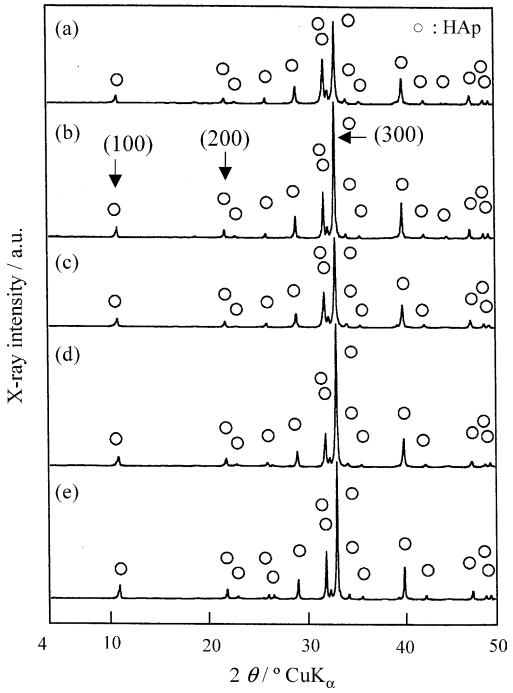

Fig. 1. XRD patterns of the products from typical starting solutions with various Ca/P ratios. (a) Ca/P ratio of 1.67, (b) 1.60, (c) 1.40, (d) 1.20 and (e) 1.00.

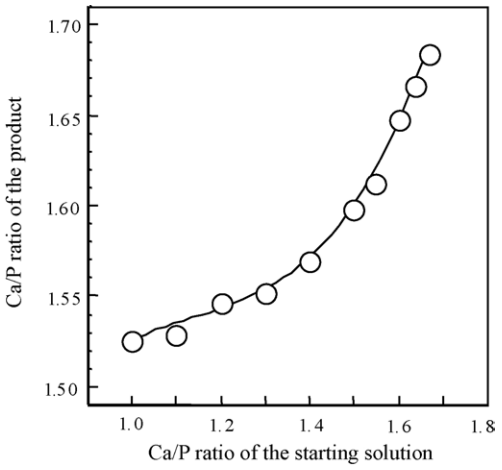

Fig. 2. Relationship between Ca/P ratio of the product and nominal Ca/P ratio of the starting solution.

tern after crushing the sample using a mortar and a pestle. In the cases of Fig. 1 (b)–(e), the products consisted of uniform apatite phase and had the XRD reflections characteristic of the (1 0 0), (2 0 0) and (3 0 0) planes. These results indicate that the present apatite gives preferred orientation in the *c*-axis direction of the hexagonal crystal, leading to develop the *a*- or *b*-plane of the apatite crystal.

The Ca/P molar ratios of the above-mentioned apatite were determined using an ICP-ES. Fig. 2 shows the relationship between Ca/P ratio of the product and nominal Ca/P ratio of the starting solution. The Ca/P ratio of the product increased with nominal Ca/P ratio of the starting solution. This result shows that the Ca/P ratio of the product can be easily controlled in the range of 1.53–1.69 by changing the Ca/P ratio of the starting solutions from 1.00–1.67.

Fig. 3 shows the FT-IR spectra of the resulting apatite with well-controlled Ca/P ratio. In the case of the Ca/P = 1.67 of the starting solution (Fig. 3(a)), the absorptions at 1300–900, 600 and 570 cm^{-1} assignable to the PO_4^{3-} groups and those at 3570 and 630 cm^{-1} assigned to the OH^- group were detected. In addition, the absorptions assignable to the CO_3^{2-} group were detected at 1600–1400 and ~880 cm^{-1} in the present investigation, as shown by the arrow marks.

As for the incorporation of CO_3^{2-} into HAp, Monma and Takahashi[20] reported as follows: (i) when the CO_3^{2-} group substitutes for the PO_4^{3-} group in the HAp (Type B of cabonate-containing HAp (CO_3HAp)), the characteristic absorptions appear at 1455, 1430, 1415 and 872 or 862 cm^{-1}; (ii) when the CO_3^{2-} group substitutes for the OH^- group in the HAp (Type A of the CO_3HAp), the absorptions appear at 1542 or 1546, 1465 and 879 or 883 cm^{-1}. As shown in Fig. 3, the present absorptions indicate that the CO_3^{2-} group substitutes for both PO_4^{3-} and OH^- groups in the HAp structure. Thus the present HAp powder can be referred to as Type AB of CO_3HAp. The formation of this CO_3HAp may be due to the generation of CO_2 through the hydrolysis of the $(NH_2)_2CO$.

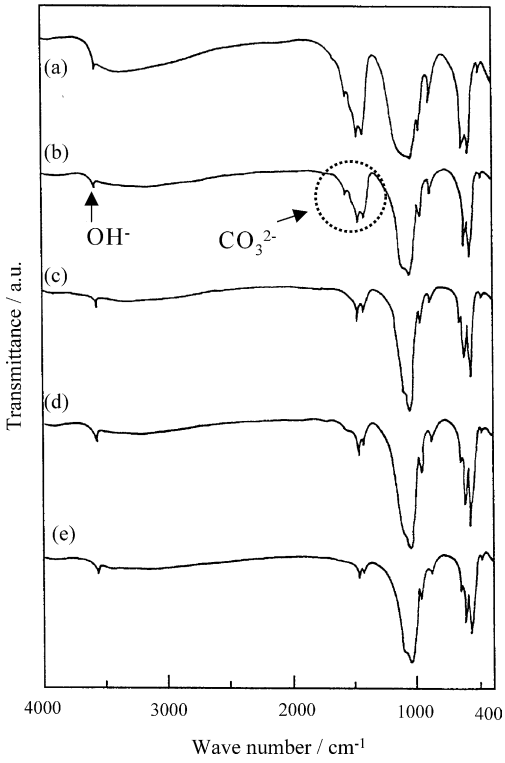

Fig. 3. FT-IR spectra of the resulting Ca-def HAp from typical starting solutions with various Ca/P ratios. (a) Ca/P ratio of 1.67, (b) 1.60, (c) 1.40, (d) 1.20 and (e) 1.00.

In the cases of Fig. 3(b)–(e), the FT-IR spectra of the resulting apatite with the lower Ca/P ratio of 1.67 are assignable to those of the typical CO_3HAp. However, the absorption assigned to the CO_3^{2-} group decreased with increasing Ca/P ratio of the resulting apatite. Thus, we performed elemental analysis of the resulting apatite in order to determine the actual carbon content. The result is shown in Fig. 4.

The figure illustrates the relationship between CO_3^{2-} content of the resulting apatite and Ca/P ratio of the product. The

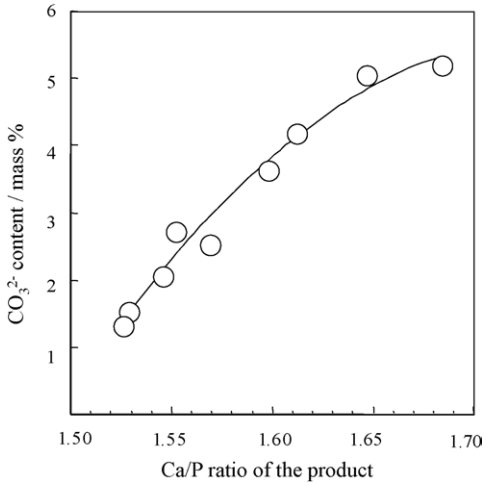

Fig. 4. Relationship between CO_3^{2-} content and Ca/P ratio of the Ca-def HAp.

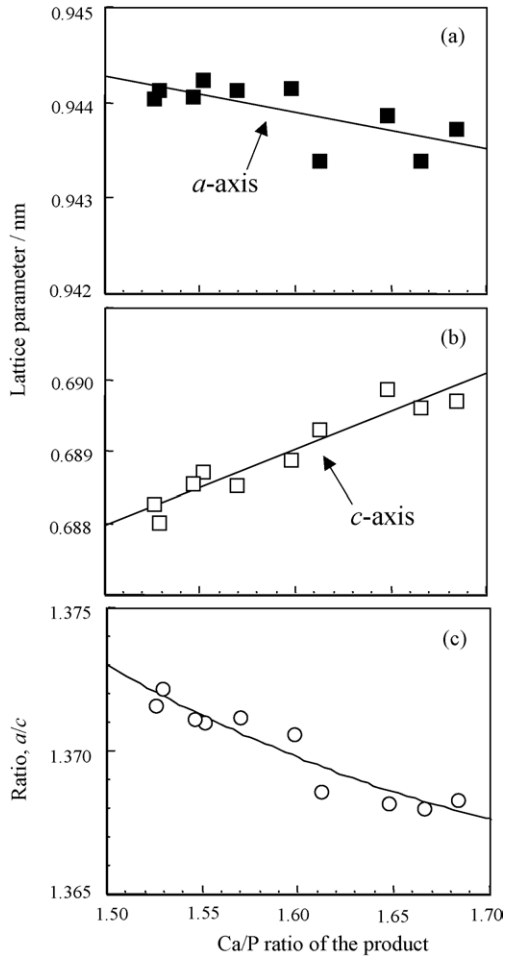

Fig. 5. Lattice parameters of the *a*-axis (a) and *c*-axis (b) and the *a*/*c* ratio (c) against the Ca/P ratio of the Ca-def HAp.

CO_3^{2-} content of the resulting apatite increased from ~1 to ~5 mass% with the Ca/P ratio of the product. Both results of FT-IR and elemental analysis show that the incorporation of CO_3^{2-} into apatite structure is depressed by decreasing the Ca/P ratio of the starting solution.

The above-mentioned phenomena suggest that, when the Ca/P ratio of the starting solution is less than 1.67, HPO_4^{2-} will be incorporated into the PO_4^{3-} site of the apatite structure to compensate the charge imbalance caused by the lack of Ca^{2+} ions. Although many CO_3^{2-} ions are also incorporated into the PO_4^{3-} site of the HAp structure, the HPO_4^{2-} ions will be easier to incorporate into HAp structure than the CO_3^{2-} ions in the experimental conditions if one takes the solubility products of $CaCO_3$ and HAp into account. Thus, the CO_3^{2-} contents in the Ca-def HAp may decrease with decreasing Ca/P ratio of the starting solution.

Next, we measured the lattice parameters of the *a*-axis and the *c*-axis. The results are shown in Fig. 5(a) and (b), together with the *a*/*c* ratio (Fig. 5(c)). With increasing Ca/P ratio of the resulting apatite, the lattice parameter of the *a*-axis slightly decreased, while that of the *c*-axis increased. In addition, the *a*/*c* ratio decreased with increasing Ca/P ratio of the resulting apatite.

According to Elliott,[21] the lattice parameters of crystalline Ca-def HAp increase in the *a*-axis direction with decreasing Ca/P ratio, but decrease in the *c*-axis direction. Thus, the *a*/*c* ratio increases with a decrease in the Ca/P ratio. The present result is consistent with the above findings. The increase in the *a*-axis parameter with decreasing Ca/P ratio may be due to more incorporation of HPO_4^{2-} ion into Ca-def HAp structure.

3.2. Morphologies of the resulting calcium-deficient apatite fibres

Fig. 6 shows that SEM micrographs of the apatite synthesized from starting solutions with the Ca/P ratios of 1.00 (Fig. 6(a)), 1.40 (Fig. 6(b)) and 1.67 (Fig. 6(c)). It can be seen from these SEM observations that the resulting apatites are composed of fibre-shaped particles with long-axes of ~60 to ~100 μm. All the synthesized apatites had morphologies of such fibre shape. In addition, the short-axis size of the fibre slightly decreased with increasing Ca/P ratio. This result indicates that the aspect ratio of the fibres increases with the Ca/P ratio. Judging from these observations and the XRD results, we consider that these Ca-def HAp fibres may elongate along the direction of the *c*-axis to develop the *a*- and *b*-planes of the hexagonal crystals.

Fig. 7 shows the TEM micrograph of the typical Ca-def HAp fibres, together with the selected area electron diffraction (SAED). SAED observations were performed in four areas (A, B, C and D) along the long-axis of the fibre. The

Fig. 6. SEM micrographs of the Ca-def HAp fibres synthesized from starting solutions with the Ca/P ratios of 1.00 (a), 1.40 (b) and 1.67 (c).

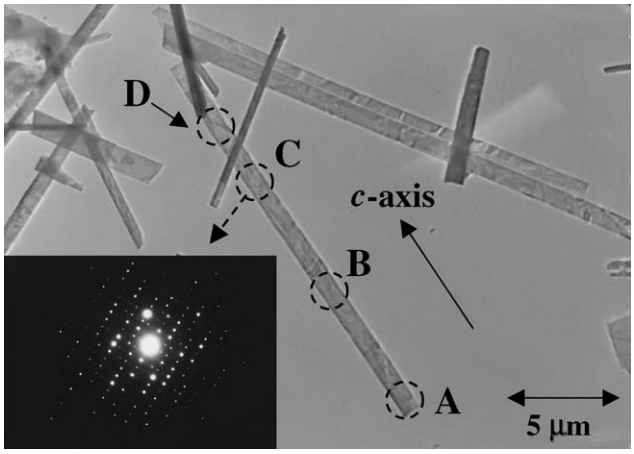

Fig. 7. TEM micrograph of typical Ca-def HAp fibres, together with the SAED pattern from area C. Synthesis conditions; (i) starting solution: Ca/P ratio of 1.50, (ii) heating temperature and time: 80 °C for 24 h and then 90 °C for 72 h.

diffraction pattern from area C showed distinct spots corresponding to an apatite structure with high crystallinity. The other diffraction patterns had similar geometry to the pattern in the area C. As all diffraction patterns showed the same geometry along the long-axis of the fibre, it was concluded that the present Ca-def HAp fibres were of single crystal.

The microstructure of the single-crystal Ca-def HAp fibres was examined on the basis of both bright and dark field images. The results are shown in Fig. 8. The bright field image (Fig. 8(a)) illustrates black contours oriented across the short axis of the fibre. In addition to the black contours, many ripples were also observed in the fibres. The contrast from these contours was also observed in dark field image (Fig. 8(b)). Tilting experiments confirmed that this contrast arose due to strain in the fibres, i.e. that they are bend contours and not defects. Our TEM observations illustrate that the fibres are highly strained single crystals.

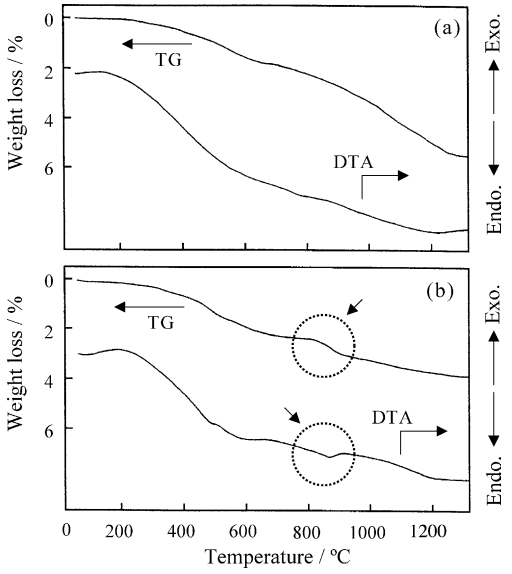

Fig. 9. DTA-TG curves of the Ca-def HAp fibres synthesized from the starting solutions with Ca/P ratios of 1.60 (a) and 1.00 (b).

We conclude that the present single-crystal Ca-def HAp fibres preferentially grow along the *c*-axis to develop the *a*(*b*)-plane of the hexagonal HAp.

3.3. Thermal stability of the resulting calcium-deficient apatite fibres

The phase changes of the Ca-def HAp during heating were examined using DTA-TG and XRD. Fig. 9 shows the DTA-TG curves of the Ca-def HAp fibres synthesized from the starting solutions with the Ca/P ratios of 1.60 (Fig. 9(a)) and 1.00 (Fig. 9(b)). The actual Ca/P ratios of the prepared Ca-def HAp fibres were 1.65 and 1.53, respectively. In Fig. 9(a), the TG curve demonstrates a continuous weight loss above 200 °C, while the DTA curve shows an endothermic

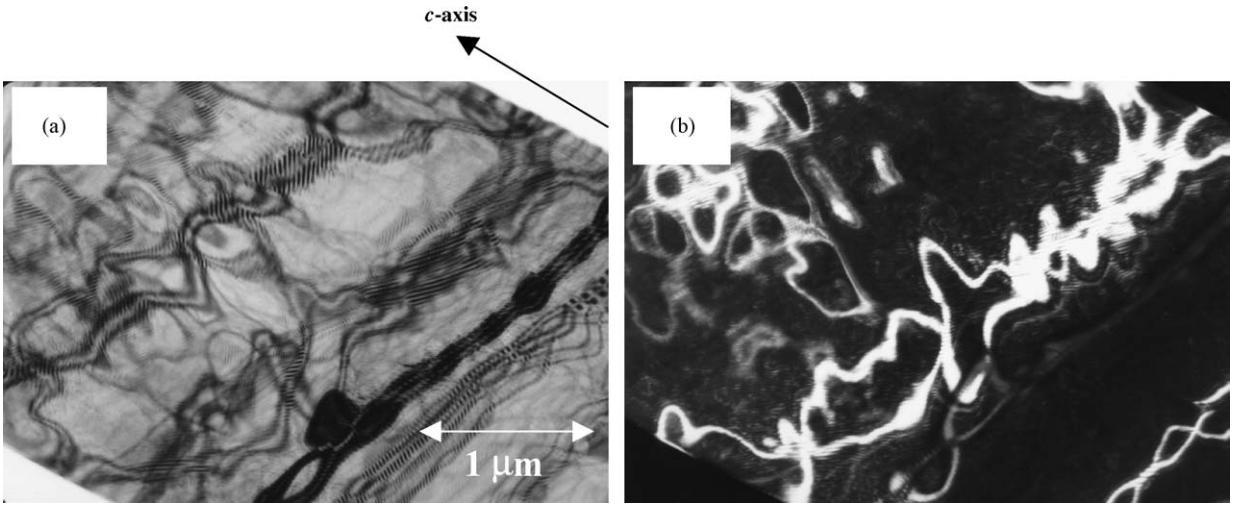

Fig. 8. TEM micrographs of the Ca-def HAp fibres synthesized from starting solutions with the Ca/P ratio of 1.50. (a) Bright- and (b) dark-field imaging.

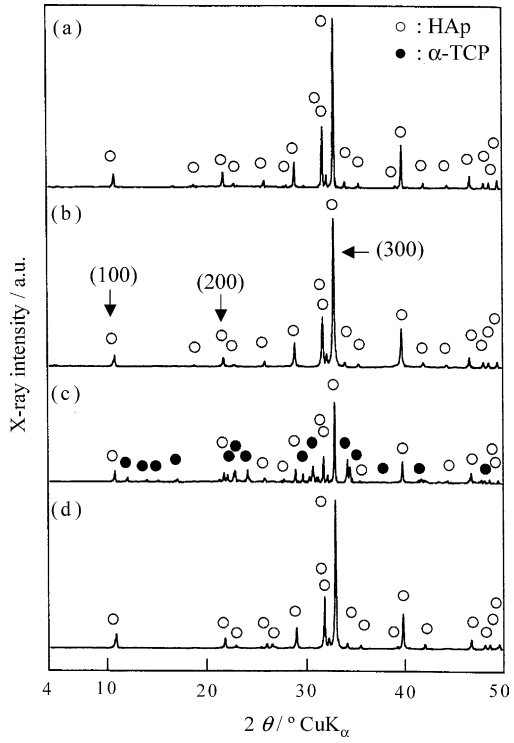

Fig. 10. XRD pattern of the Ca-def HAp fibres before (b, d) and after heat treatment at 1200 °C for 1 h (a, c); (a, b) Ca-def HAp fibres synthesized from the starting solution with the Ca/P ratio of 1.60 and (c, d) the Ca/P ratio of 1.00.

change over the measured temperature range. This apparent endothermic change may be due only to the drift of the base line.

In the case of Fig. 9 (b), the TG curve shows the weight loss in the range of 800–1000 °C, as pointed by the arrow mark. The DTA curve also shows an endothermic reaction in the range of 800–1000 °C, corresponding to the weight loss of the TG curve. These weight loss and endothermic reaction may be due to the decomposition of the Ca-def HAp into the TCP.

Fig. 10 shows the XRD pattern of the Ca-def HAp fibres before (Fig. 10(b and d)) and after heat treatment at 1200 °C for 1 h (Fig. 10(a and c)). These testing samples correspond to those of the DTA-TG measurement. Fig. 10(a) and (b) show the XRD patterns of the Ca-def HAp fibres synthesized from the starting solution with the Ca/P ratio of 1.60. These XRD patterns show that the testing samples consisted of apatite single phase, which has preferred orientation in the *c*-axis direction, and that no changes occurred in the crystalline phase during heat treatment. On the other hand, in the case of Fig. 10(c) and (d), the single apatite phase was present in the sample before the heat treatment, while the HAp/TCP biphase present in the heated sample. These results indicate that the present Ca-def HAp fibre technology will be effective for creating the biodegradable materials consisting of TCP phase or TCP/HAp biphase.

4. Conclusions

Calcium-deficient apatite (Ca-def HAp) fibres were successfully synthesized by a homogeneous precipitation method using starting solutions with Ca/P ratio of 1.00–1.67. In the case of the Ca/P ratio of 1.67, the resulting apatite fibre had long-axes of about 60–100 μm and contained 5.2 mass% of carbonate ions. The Ca/P ratio of the apatite fibres could be controlled in the range of 1.53–1.68 by changing the Ca/P ratio of the starting solutions from 1.00 to 1.67. The long-axes and the carbonate contents of the resulting calcium-deficient apatite fibres increased with the Ca/P ratio of the starting solutions. These apatite fibres were of single crystal and had a preferred orientation in the *c*-axis direction. The resulting Ca-def HAp fibres were decomposed to form the HAp/TCP biphase. The present technology will be effective for creating the biodegradable materials consisting of TCP phase or TCP/HAp biphase.

References

1. Hench, L. L., Bioceramics. *J. Am. Ceram. Soc.*, 1998, **81**, 1705–1728.
2. Hench, L. L., Bioceramics: For concept to clinic. *J. Am. Ceram. Soc.*, 1991, **74**, 1487–1510.
3. Kawasaki, T., Hydroxyapatite as a liquid chromatographic packing. *J. Chromatogr.*, 1991, **544**, 147–184.
4. Ioku, K., Yoshimura, M. and Somiya, S., Hydrothermal synthesis of ultrafine hydroxyapatite single crystals. *Nihon-Kagaku-Kaishi*, 1988, **1988**, 1565–1570.
5. Nagata, F., Yokogawa, Y., Toriyama, M., Kawamoto, Y., Suzuki, T. and Nishizawa, K., Hydrothermal synthesis of hydroxyapatite crystals in the presence of methanol. *J. Ceram. Soc. Jpn.*, 1995, **103**, 70–73.
6. Aizawa, M., Kinoshita, M., Yamada, K., Itatani, K. and Kishioka, A., Effects of synthesis and morphology of carbonate-containing hydroxyapatite prepared by homogeneous precipitation method. *Inorg. Mater.*, 1998, **5**, 387–397.
7. Aizawa, M., Howell, F. S., Itatani, K., Yokogawa, Y., Nishizawa, K., Toriyama, M. *et al.*, Fabrication of porous ceramics with well-controlled open pores by sintering of fibrous hydroxyapatite particles. *J. Ceram. Soc. Jpn.*, 2000, **108**, 249–253.
8. Aizawa, M., Porter, A. E., Best, S. M. and Bonfield, W., High resolution transmission electron microscopy investigation of single crystal apatite fibres synthesized by a homogeneous precipitation method. *Key Eng. Mater.*, 2003, **240–242**, 509–512.
9. Aizawa, M., Porter, A. E., Best, S. M. and Bonfield, W., Microstructual changes of single-crystal apatite fibres during heat treatment. *Key Eng. Mater.*, 2004, **254–256**, 915–918.
10. Kawata, M., Uchida, H., Itatani, K., Okada, I., Koda, S. and Aizawa, M., Development of porous ceramics with well-controlled porosities and pore sizes from apatite fibers and their evaluations. *J. Mater. Sci. Mater. Med.*, 2004, **15**, 817–823.
11. Aizawa, M., Tsuchiya, Y., Itatani, K., Suemasu, H., Nozue, A. and Okada, I., Fabrication of hybrid materials by the introduction of poly(methylmethacrylate) into the porous hydroxyapatite ceramics. *Bioceramics*, 1999, **12**, 453–456.
12. Aizawa, M., Ito, M., Itatani, K., Suemasu, H., Nozue, A., Okada, I. *et al.*, In vivo and in vitro evaluation of the biocompatibility of the hydroxyapatite-PMMA hybrid materials having mechanical property similar to that of cortical bone. *Key Eng. Mater.*, 2001, **218–220**, 465–468.

13. Aizawa, M., Ito, M., Itatani, K., Okada, I. and Matsumoto, M., Development of bioactive tailor-made materials by inorganic/organic hybridization. *Phosphor. Lett.*, 2003, **46**, 7–14.
14. Aizawa, M., Ueno, H., Itatani, K. and Okada, I., Development of scaffolds for tissue engineering using single-crystal apatite fibres and their biological evaluation by osteoblastic cell. *Trans. Mater. Res. Soc. Jpn.*, 2003, **28**, 849–852.
15. Aizawa, M., Shinoda, H., Uchida, H., Itatani, K., Okada, I., Matsumoto, M. *et al.*, Development and biological evaluation of apatite fiber scaffolds with large pore size and high porosity for bone regeneration. *Key Eng. Mater.*, 2003, **240–242**, 647–650.
16. Aizawa, M., *Culture Method of Osteoblast*, Japan patent Tokukai 2003-93052, 2 April, 2003.
17. Kreidler, E. R. and Hummel, F. A., The crystal chemistry of apatite: structure fields of fluor- and chloroapatite. *Am. Mineral.*, 1970, **55**, 170–184.
18. Monma, H., Ueno, S. and Kanazawa, T., Properties of hydroxyapatite prepared by the hydrolysis of tricalcium phosphate. *J. Chem. Tech. Biotechnol.*, 1981, **31**, 15–24.
19. Irie, H., Bone substitute to be remodeled to natural bone. *Bull. Ceram. Soc. Jpn.*, 2003, **38**, 55–57.
20. Monma, H. and Takahashi, T., Preparation and thermal changes of carbonate-containing apatite. *Gypsum Lime*, 1987, **210**, 287–291.
21. Elliott, J. C., *Structure and Chemistry of the Apatites and other Calcium Orthophosphates*. Amsterdam-London-New York-Tokyo, Elsevier, 1994, pp. 151–52.